Radiomics for the non-invasive prediction of the BRAF mutation status in patients with melanoma brain metastases

Anna-Katharina Meißner[1]*, Robin Gutsche[2,3]*, Norbert Galldiks[2,4,5]*, Martin Kocher[2,6], Stephanie T. Jünger[1], Marie-Lisa Eich[7], Manuel Montesinos-Rongen[8], Anna Brunn[8], Martina Deckert[5,8], Christina Wendl[9], Wolfgang Dietmaier[10], Roland Goldbrunner[1,5], Maximilian I. Ruge[5,6], Cornelia Mauch[5,11], Nils-Ole Schmidt[12], Martin Proescholdt[12], Stefan Grau[1,5], and Philipp Lohmann[2,6]

*authors contributed equally

[1]*Center for Neurosurgery, Dept. of General Neurosurgery, Faculty of Medicine and University Hospital Cologne, University of Cologne, Cologne, Germany*

[2]*Inst. of Neuroscience and Medicine (INM-3, -4), Research Center Juelich, Juelich, Germany*

[3]*RWTH Aachen University, Aachen, Germany*

[4]*Dept. of Neurology, Faculty of Medicine and University Hospital Cologne, University of Cologne, Cologne, Germany*

[5]*Center for Integrated Oncology (CIO), Universities of Aachen, Bonn, Cologne and Duesseldorf, Cologne, Germany*

[6]*Center for Neurosurgery, Dept. of Stereotactic and Functional Neurosurgery, Faculty of Medicine and University Hospital Cologne, University of Cologne, Cologne, Germany*

[7]*Dept. of Pathology, Faculty of Medicine and University Hospital Cologne, University of Cologne, Cologne, Germany*

[8]*Inst. of Neuropathology, Faculty of Medicine and University Hospital Cologne, Cologne, Germany*

[9]*Dept. of Radiology and Division of Neuroradiology, University Hospital Regensburg, Germany*

[10]*Inst. of Pathology and Molecular Pathology Diagnostic Unit, University Hospital Regensburg, Regensburg, Germany*

[11]*Dept. of Dermatology, Faculty of Medicine and University Hospital Cologne, University of Cologne, Cologne Germany*

[12]*Dept. of Neurosurgery, University Hospital Regensburg, Regensburg, Germany*

Running title: Prediction of BRAF mutation using MRI radiomics

CORRESPONDENCE

Philipp Lohmann, PhD

Institute of Neuroscience and Medicine (INM-4)

Research Center Juelich

52425 Juelich

Germany

Email: p.lohmann@fz-juelich.de

Phone: +49 2461 6196357

Fax: +49 2461 612302

FUNDING

This work was supported by the Deutsche Forschungsgemeinschaft (DFG, German Research Foundation; project number 428090865/SPP 2177; R.G., N.G., and P.L.).

CONFLICT OF INTEREST

The authors declare no conflicts of interest.

AUTHORSHIP

Experimental design: AKM, RG, NG, PL

Implementation: All

Analysis and interpretation of data: AKM, RG, NG, MP, SG, PL

Writing of the manuscript and approval of final version: All

WORD COUNT

Abstract: 250

Manuscript body: 3,109

Total: 5,055

Number of figures/tables: 6

References: 33

ABSTRACT

Background: The BRAF V600E mutation is present in approximately 50% of patients with melanoma brain metastases and an important prerequisite for response to targeted therapies, particularly BRAF inhibitors. As heterogeneity in terms of BRAF mutation status may occur in melanoma patients, a wild-type extracranial primary tumor does not necessarily rule out a targetable mutation in brain metastases using BRAF inhibitors. We evaluated the potential of MRI radiomics for a non-invasive prediction of the intracranial BRAF mutation status.

Methods: Fifty-nine patients with melanoma brain metastases from two university brain tumor centers (group 1, 45 patients; group 2, 14 patients) underwent tumor resection with subsequent genetic analysis of the intracranial BRAF mutation status. Preoperative contrast-enhanced MRI was manually segmented and analyzed. Group 1 was used for model training and validation, group 2 for model testing. After radiomics feature extraction, a test-retest analysis was performed to identify robust features prior to feature selection. Finally, the best performing radiomics model was applied to the test data. Diagnostic performances were evaluated using receiver operating characteristic (ROC) analyses.

Results: 22 of 45 patients (49%) in group 1, and 8 of 14 patients (57%) in group 2 had an intracranial BRAF V600E mutation. A linear support vector machine classifier using a six-parameter radiomics signature yielded an area under the ROC curve of 0.92 (sensitivity, 83%; specificity, 88%) in the test data.

Conclusions: The developed radiomics classifier allows a non-invasive prediction of the intracranial BRAF V600E mutation status in patients with melanoma brain metastases with high diagnostic performance.

KEYWORDS

Machine learning; artificial intelligence (AI); radiogenomics; MRI; brain tumors

KEY POINTS

- MRI radiomics predicts non-invasively the intracranial BRAF V600E mutation status in patients with melanoma brain metastases with high diagnostic performance
- The developed radiomics model based on routinely acquired structural MRI can be easily implemented in clinical routine
- Considering the heterogeneity between the BRAF mutation status of the extracranial primary tumor and a metastatic brain lesion in melanoma patients, the developed model is of value for personalized treatment decisions, e.g., the use of BRAF inhibitors

IMPORTANCE OF THE STUDY

The BRAF V600E mutation in patients with melanoma brain metastases is an important prerequisite for response to targeted therapies using BRAF inhibitors. Of note, the intracranial efficacy of these therapies may be limited by heterogeneity in terms of the BRAF mutation status between the extracranial primary tumor and the metastatic brain lesion in this group of patients. Furthermore, most patients with melanoma brain metastases are considered for radiosurgery as first-line treatment option, so that tissue samples are usually not available. The present study shows the usefulness of a machine learning model based on the combination of clinical parameters and MRI radiomics features to predict non-invasively the intracranial BRAF mutation status in patients with melanoma brain metastases with high diagnostic accuracy.

INTRODUCTION

About 40-60% of patients with stage IV melanoma develop brain metastases in the course of the disease[1]. Nearly 50% of patients with melanoma brain metastases harbor one of various mutations of the BRAF gene (v-Raf murine sarcoma viral oncogene homolog B1) [2,3]. The most frequent mutation V600E, present in about 70% of cases, comprise the substitution of valine for glutamic acid [4]. Importantly, a BRAF mutation is a prerequisite for an effective response to targeted therapies using BRAF inhibitors such as vemurafenib and dabrafenib. These agents have shown considerable intracranial response rates in clinical trials with a significant improvement of overall and progression-free survival [5-8]. Nevertheless, recent studies indicated a heterogeneity between the BRAF mutation status of the extracranial primary melanoma and melanoma brain metastases in up to 26% of patients, resulting in inefficacy of BRAF inhibitor targeted therapy in wild-type tumors [2,9,10]. Thus, knowledge of the BRAF mutation status of the brain metastases may substantially support treatment decisions.

The mutation status of melanoma brain metastases is usually defined through genetic analysis of tissue samples after tumor resection or biopsy. In most patients, melanoma brain metastases are treated at first-line by radiosurgery [8]. Therefore, tissue samples are usually available only for patients with clinically symptomatic and space-occupying brain metastases in whom surgical removal is indicated. Nevertheless, according to the most recent European guidelines of the EANO and ESMO for diagnosis, treatment, and follow-up of melanoma brain metastases, determination of the BRAF mutation status is highly recommended for all patients [8]. Thus, methods for a reliable non-invasive assessment of the intracranial BRAF mutation status are of high clinical relevance, especially in patients suitable for stereotactic radiosurgery without the need for further surgical interventions or for the use of BRAF inhibitors for the treatment of

brain metastases relapse after radiosurgery as first-line treatment option. Radiomics, a method from the broad field of Artificial Intelligence aims at the large-scale extraction of image features from routinely acquired imaging data, that are not accessible through conventional image analysis. Following radiomics feature extraction, prognostic or predictive mathematical models are developed to support clinical decision-making [11,12]. Currently, radiomics is increasingly investigated in Neuro-Oncology and demonstrated its potential for the histomolecular characterization of brain metastases [13-16].

Here, we evaluated the potential of MRI radiomics for the non-invasive diagnosis of the BRAF V600E mutation status in patients with melanoma brain metastases.

PATIENTS AND METHODS

Ethics statement

The present study was conducted according to the guidelines of the declaration of Helsinki, and the retrospective analysis of data was approved by the Ethics Committees of the University Hospital Cologne, Germany, (approval number 19-1686) and the University Hospital Regensburg, Germany (approval number 20-1799-101).

Patients

From 2010 to 2020, we retrospectively identified patients with melanoma brain metastases from the Brain Tumor Centers of the University Hospitals Cologne and Regensburg, Germany, who (i) had no previous local treatment, (ii) underwent preoperative contrast-enhanced MRI, (iii) had a known intrametastatic BRAF V600E mutation status based on the genetic analysis of tissue samples after surgical brain metastasis resection.

Clinical data were obtained from an electronic database and patient files. We recorded gender, age, previous systemic therapy, time from first diagnosis to the development of brain metastases, number, volume, and localization of brain metastases, clinical symptoms, preoperative Karnofsky performance status, and the BRAF V600E mutation status of the extracranial tumor and the brain metastases.

Genetic analysis of BRAF V600E mutation status

DNA was extracted from formalin-fixed, paraffin-embedded (FFPE) specimens of patients with morphologically and immunohistochemically (vimentin+, S100 protein+, Melan-A+, HMB45+) proven brain metastases of systemic malignant melanoma. The

BRAF V600E mutation status was analyzed in the University Hospital Cologne as follows:

DNA was subjected to polymerase chain reaction (PCR) for hot spot (V600E, K, R) mutation of the BRAF gene (BRAF-F: 5'-AAGACCTCACAGTAAAAATAGGTG-3'; BRAF-R: 5'-Biotin-AATCAGTGGAAAAATAGCCTCAAT-3'; 134 bp from 140753245 to 140753378, according to NC_000007.14 (GRCh38.p13) under https://www.ncbi.nlm.nih.gov/nuccore). PCR products were analyzed by QIAxcel Advanced system (Qiagen, Hilden, Germany) followed by pyrosequencing (BRAF-S: 5'-GTGATTTTGGTCTAGCTAC-3').

The BRAF V600E mutation status was analyzed in the University Hospital Regensburg following the approach described by Kriegl and colleagues [17]. In brief, 40 ng DNA were amplified by PCR using the following primer sequences: 5'-TGAAGACCTCACAGTAAAAATAGG-3' and 5`-Biotin-TCCAGACAACTGTTCAAACTG-3'. As sequencing primer, 5'-GTAAAAATAGGTGATTTTGG-3' was used.

In both centers, sequencing results were analyzed by the PyroMark Q24 software (Qiagen, Hilden, Germany) according to the instructions of the provider.

MR imaging

Structural MR imaging used in this study was limited to T1-weighted contrast-enhanced, and T2-weighted sequences only. Preoperative structural T1-weighted non-contrast and FLAIR MR images were not available for the radiomics analysis.

Image preprocessing and definition of tumor mask

Image preprocessing was performed using the FSL toolbox version 5.0 (FMRIB Software Library, http://www.fmrib.ox.ac.uk/fsl) [18] the MIC-DKFZ HD-BET brain extraction tool (https://github.com/MIC-DKFZ/HD-BET) [19], the Advanced Normalization Tools ANTS version 2.1 (http://stnava.github.io/ANTs) [20], and the open source image analysis software ITK SNAP version 3.6 (http://www.itksnap.org/) [21] following the conversion of all images to NifTI format (dcm2niix, https://github.com/rordenlab/dcm2niix) [22]. After rigid co-registration of the T2-weighted MRI to the T1-weighted contrast-enhanced MRI using FSL-FLIRT (FMRIB's Linear Image Registration Tool) and brain extraction using HD-BET, a nonparametric normalization algorithm for the removal of low frequency intensity nonuniformities (bias field) in the MR images was performed using N4ITK [23]. MR image intensities were Z-Score normalized according to current recommendations [24] prior to manual tumor segmentation based on the volume of contrast enhancement using ITK-SNAP. Missing voxels and small holes in the resulting tumor masks were augmented by the FSLmaths hole-filling algorithm.

Radiomics feature extraction

Radiomics feature extraction was performed using the open-source package PyRadiomics (version 3.0.1) in Python (https://pyradiomics.readthedocs.io/en/latest/) [25]. Prior to extraction, images were resampled to 1 mm^3 voxel size and discretized to a bin width of 0.1. Three basic groups of radiomics features were extracted, including 16 shape, 19 first order and 75 second order features subdivided by the underlying gray level matrices, i.e., gray level co-occurrence matrix (GLCM), gray level dependence matrix (GLDM), gray level run length matrix (GLRLM), gray level size zone matrix (GLSZM), and neighboring gray tone difference matrix (NGTDM). Features

were calculated on the original image and after applying wavelet and Laplacian of Gaussian (LoG) filter methods, which resulted in a total of 1,316 radiomics features per imaging sequence.

Test-retest analysis and feature selection

To avoid the usage of non-robust radiomics features, we followed the conceptual framework proposed by Zwanenburg and colleagues [26]. We used the image perturbation method chain translation, noise, and volume adaption to produce an augmented version of the original image. In a test-retest approach, radiomics features were calculated and compared for both images. Repeatability between features was evaluated by the intraclass correlation coefficient (ICC). Features were considered repeatable if the lower and upper limits of the ICC 95% confidence interval were in the range of 0.91 to 1.00. The ICC analysis was implemented in Python (Pingouin, version 0.3.9) [27]. Following this analysis, the 100 radiomics features with highest mutual information were selected for model training.

Model training and testing

Prior to training different classification models, the training set (patient group 1, University Hospital Cologne) was split into a training and a validation set. All radiomics features were standardized by subtracting the mean and dividing by the standard deviation of the training data. A 10-fold stratified cross-validation (70% training, 30% validation) was performed with subsequent feature selection based on their averaged feature importance rankings across all subsets of the data. This process was repeated until the average validation metric did not improve further and the model with the best performing features and hyperparameters was retrained on the complete training data set. Finally, the best performing model in the training data was applied to the external

test data set (patient group 2, University Hospital Regensburg). Importantly, the final model testing was performed blinded to the BRAF mutation status. Afterwards, the classification results were transferred to the University Hospital Regensburg and the diagnostic performance of the classifier was assessed fully independent from the researchers involved in model generation. The radiomics workflow is presented in Figure 1.

The prediction of the BRAF mutation status was derived from three individual models. Model 1 was based on the patient age only. Model 2 and Model 3 were trained on a combination of the patient age and radiomics features. Whereas Model 2 included radiomics features from contrast-enhanced T1-weighted MRI only, Model 3 included features from both contrast-enhanced T1- and T2-weighted MR images. All processing steps were implemented in Python (sklearn, version 0.24.1).

Feature map extraction

In order to evaluate the local radiomics feature expression and to visualize potential feature patterns for tumor classification, we adapted the procedure by Vuong and colleagues [28]. For image patches of 3x3x3 voxels, local radiomics features were calculated on the volume of interest.

Statistical analysis

Descriptive statistics are provided as mean and standard deviation or median and range. The diagnostic performance of each classifier was evaluated by receiver operating characteristics analysis. To avoid experimental bias, the statistical analysis of the external test data (patient group, University Hospital Regensburg) was performed by an independent researcher not involved in the model generation.

Significant differences between features were tested using the two-tailed Student's t-test, with previous confirmation of a normal distribution by the Shapiro-Wilk test. P-values of 0.05 or less were considered statistically significant. Statistical analyses were implemented in Python (Pingouin, version 0.3.9) [27].

RESULTS

Patient and clinical characteristics

Fifty-nine patients from two University Hospitals were retrospectively identified, thereof 45 patients from the Brain Tumor Center of the University Hospital Cologne, Germany (mean age, 60 ± 12 years; age range, 39 - 83 years; 21 females, 24 males). One patient received the corticosteroid dexamethasone prior to preoperative MRI (dosage, 4 mg/day for 12 days). Twenty-three patients had melanoma brain metastases harboring a BRAF mutation, 22 patients were BRAF wild-type. Six patients (13%) showed a discrepancy of the BRAF mutation status between the extracranial tumor and the melanoma brain metastasis.

Fourteen patients with surgically resected melanoma brain metastases were identified at the Brain Tumor Center of the University Hospital Regensburg, Germany (mean age, 59 ± 11 years; age range, 42 - 76 years; 6 females, 8 males). Eight patients had melanoma brain metastases harboring a BRAF mutation, 6 patients had a BRAF wild-type. Discordance of extra- and intracranial BRAF mutation status was present in 2 patients (14%).

Patients with a BRAF mutation were significantly younger than those with a BRAF wild-type (53 ± 10 vs. 65 ± 9 years; $p<0.001$). No statistically significant differences were found in patients' sex, anatomical location, tumor volume, presence of intratumoral hemorrhage or tumor cysts of the brain metastases. Patient characteristics are summarized in Table 1.

Classification results

Three individual models were compared in their ability to predict the BRAF mutation status in patients with melanoma brain metastases. Model 1 classified patients below the age of 59 as BRAF mutated with an area under the receiver operating characteristic curve (AUC) of 0.80 (sensitivity, 72%; specificity, 78%; accuracy, 78%) in the training set and with an AUC of 0.58 (sensitivity, 50%; specificity, 63%; accuracy, 57%) in the test set.

The best classification of the BRAF mutation status was achieved by combining clinical and radiomics features calculated on contrast-enhanced T1-weighted MRI using a linear support vector machine classifier (model 2). Five radiomics features and the patients' age were included in the final model. The model achieved an average AUC of 0.87 ± 0.09 in the stratified 10-fold cross validation of the training data (mean sensitivity, 79 ± 15%; mean specificity, 91 ± 10%, mean accuracy, 85 ± 10%). In the test data, the model yielded an AUC of 0.92 (sensitivity, 83%; specificity, 88%; accuracy, 86%).

Integration of radiomics features calculated from T2-weighted MRI in the training process resulted in a linear support vector machine classifier based on seven radiomics features and the patients' age (model 3). The training performance resulted in a mean AUC of 0.92 ± 0.80 (mean sensitivity, 86 ± 13%; mean specificity, 93 ± 10%; mean accuracy, 89 ± 8%.). The classifier achieved an AUC of 0.81 (sensitivity, 100%; specificity, 75%; accuracy, 88) in the test data. Due to missing MRI data, only eight patients were included in the test data set of model 3.

The results are summarized in Figure 2 and Table 2.

Feature importance

The feature importance expressed as support vector machine coefficients for model 2 and model 3 are shown in Figure 3. In both models, the patient age contributed the most to the decision function of the classifier. Interestingly, the second most contributing feature in model 2, the inverse difference moment of the grey level co-occurrence matrix (GLCM) calculated on Laplacian of Gaussian filtered contrast-enhanced T1-weighted MRI was significantly different between BRAF wild-type and BRAF mutant patients in the test set ($p<0.05$). Representative local feature expression differences between BRAF wildtype and BRAF mutant melanoma brain metastases are shown in Figure 4.

DISCUSSION

One main finding of the present study is that a machine learning model based on a combination of clinical parameters and MRI radiomics features predicts the intracranial BRAF V600E mutation status in patients with melanoma brain metastases with a high diagnostic accuracy, i.e., an AUC of 0.92. Furthermore, the developed model was evaluated in an albeit small, but independent test data set from another brain tumor center. Importantly, the validation of its high diagnostic performance in this data set indicates the capability of providing reliable results regardless of the used scanners and imaging parameters. Since the radiomics model is based on routinely acquired structural MRI and the developed model can be applied fully automated on a conventional computer in a few minutes, the approach seems to be applicable in clinical routine.

The usefulness of radiomics for the prediction of genomic alterations such as a BRAF mutation in patients with melanoma brain metastases has already been reported earlier by Shofty and colleagues [16]. In that study and contrast to the present results, the developed model achieved an AUC of 0.78 for the prediction of an intracranial BRAF mutation. Additionally, besides the lower prediction performance, the developed classifier was not evaluated in an external test dataset. Moreover, to reduce the risk of overfitting in accordance with published recommendations, we limited the number of radiomics features to six [29,30].

A reliable method for the non-invasive determination of the intrametastatic BRAF status is of particular clinical relevance. Importantly, recent findings indicate a discrepancy between the BRAF mutation status of the extracranial primary tumor and brain metastases in about 15% of melanoma patients, resulting in a lack of intracranial

response to BRAF inhibitors in wild-type brain metastases [9,10]. In our study, 14% of patients showed a discrepancy of the BRAF V600E mutation between the extracranial primary tumor and the metastatic brain lesions. Furthermore, in most patients with melanoma brain metastases, radiosurgery is considered as first-line treatment option, so that tissue samples are usually not available, and the intrametastatic BRAF mutation status remains unknown. In addition, the BRAF mutation status might change over time [10], leading to uncertainty even in patients from whom tissue samples are available for genetic analysis. Thus, the non-invasive evaluation of the intrametastatic BRAF mutation status appears to be beneficial for treatment decisions, i.e., the use of BRAF inhibitors.

Another main finding of our study is that the addition of MRI radiomics features to the clinical parameter age increased the diagnostic performance by more than 30%. Thus, radiomics features may be considered an additional source of diagnostic information in order to improve brain tumor diagnostics, especially in combination with already available clinical parameters. This observation is also in line with results of previous studies. For example, radiomics features derived from PET using the radiolabeled amino acid *O*-(2-[^{18}F]fluoroethyl)-L-tyrosine combined with MRI radiomics suggested a high clinical value for the differentiation of radiation-induced changes from brain metastases relapse. Importantly, the combined analysis revealed a higher diagnostic accuracy than either modality alone [31]. Furthermore, Mouraviev and co-workers proved the feasibility of radiomics for the prediction of local control after radiosurgery of brain metastases [32]. In that study, the combination of clinical parameters with radiomics features resulted in an almost 20% higher AUC compared to clinical parameters alone.

Except the evaluation of radiomics for various clinical applications (e.g., refinement of diagnostics in brain tumor patients), the evaluation of the biological meaning of radiomics features is also currently under investigation [33]. In our study, we observed that the radiomics feature inverse difference moment of the GLCM was of considerable importance for the prediction of the BRAF mutation status. This feature reflects local image homogeneity and showed high values for BRAF wild-type and low values for BRAF mutant melanoma brain metastases. Interestingly, this finding is also supported by the visual impression that BRAF mutant melanoma brain metastases show a more heterogenous pattern of contrast enhancement compared to the BRAF wild-type metastases (Figure 4). Nevertheless, further efforts are needed for a deeper understanding of radiomics features and machine learning models. This might be key for a successful translation and acceptance of radiomics into clinical practice. To obtain this goal, correlation of imaging features with spatially correlated tissue samples including extensive neuropathological work-up is necessary.

To validate our encouraging initial results, further modifications of the study design are needed. The developed radiomics model is based on structural MRI and does not include advanced MRI sequences such as T2* or diffusion-weighted imaging. Future studies should therefore investigate whether the model performance can be further increased by including advanced MRI sequences or other imaging modalities such as PET. Another point is that a potential influence of a systemic therapy (e.g., combined checkpoint blockade using ipilimumab and nivolumab) for the treatment of the primary extracranial melanoma on the radiological features of brain metastases cannot be ruled out, although only patients with newly diagnosed melanoma brain metastases were investigated in the present study. Nevertheless, the non-invasive prediction of

the BRAF mutation status using the innovative radiogenomics approach is an important clinical application.

In addition, our results should be confirmed prospectively with a higher number of patients enrolled from multiple centers. That would considerably help to increase the generally low availability of melanoma brain metastases tissue for BRAF genotyping.

In summary, our study suggests that the developed radiomics classifier is of clinical value for a non-invasive prediction of the intracranial BRAF V600E mutation status in patients with melanoma brain metastases. In addition, the radiomics model is based on routinely acquired and easily accessible structural MRI, which facilitates the implementation in clinical routine. Considering the reported heterogeneity between intra- and extracranial BRAF mutation status, the radiomics model may add valuable information for personalized treatment decision-making, i.e., the use of BRAF inhibitors.

FUNDING

This work was supported by the Deutsche Forschungsgemeinschaft (DFG, German Research Foundation; project number 428090865/SPP 2177; R.G., N.G., and P.L.).

REFERENCES

1. Ostrom QT, Wright CH, Barnholtz-Sloan JS. Brain metastases: epidemiology. *Handb Clin Neurol.* 2018; 149:27-42.

2. Heinzerling L, Baiter M, Kuhnapfel S, et al. Mutation landscape in melanoma patients clinical implications of heterogeneity of BRAF mutations. *Br J Cancer.* 2013; 109(11):2833-2841.

3. Westphal D, Glitza Oliva IC, Niessner H. Molecular insights into melanoma brain metastases. *Cancer.* 2017; 123(S11):2163-2175.

4. Soffietti R, Ahluwalia M, Lin N, Ruda R. Management of brain metastases according to molecular subtypes. *Nat Rev Neurol.* 2020; 16(10):557-574.

5. Rulli E, Legramandi L, Salvati L, Mandala M. The impact of targeted therapies and immunotherapy in melanoma brain metastases: A systematic review and meta-analysis. *Cancer.* 2019; 125(21):3776-3789.

6. Soffietti R, Abacioglu U, Baumert B, et al. Diagnosis and treatment of brain metastases from solid tumors: guidelines from the European Association of Neuro-Oncology (EANO). *Neuro Oncol.* 2017; 19(2):162-174.

7. van Opijnen MP, Dirven L, Coremans IEM, Taphoorn MJB, Kapiteijn EHW. The impact of current treatment modalities on the outcomes of patients with melanoma brain metastases: A systematic review. *Int J Cancer.* 2020; 146(6):1479-1489.

8. Le Rhun E, Guckenberger M, Smits M, et al. EANO-ESMO Clinical Practice Guidelines for diagnosis, treatment and follow-up of patients with brain metastasis from solid tumours. *Ann Oncol.* 2021.

9. Hannan EJ, O'Leary DP, MacNally SP, et al. The significance of BRAF V600E mutation status discordance between primary cutaneous melanoma and brain metastases: The implications for BRAF inhibitor therapy. *Medicine (Baltimore).* 2017; 96(48):e8404.

10. Valachis A, Ullenhag GJ. Discrepancy in BRAF status among patients with metastatic malignant melanoma: A meta-analysis. *Eur J Cancer.* 2017; 81:106-115.

11. Gillies RJ, Kinahan PE, Hricak H. Radiomics: Images Are More than Pictures, They Are Data. *Radiology.* 2016; 278(2):563-577.

12. Lohmann P, Galldiks N, Kocher M, et al. Radiomics in neuro-oncology: Basics, workflow, and applications. *Methods.* 2020.

13. Artzi M, Bressler I, Ben Bashat D. Differentiation between glioblastoma, brain metastasis and subtypes using radiomics analysis. *J Magn Reson Imaging.* 2019; 50(2):519-528.

14. Kniep HC, Madesta F, Schneider T, et al. Radiomics of Brain MRI: Utility in Prediction of Metastatic Tumor Type. *Radiology.* 2019; 290(2):479-487.

15. Ortiz-Ramon R, Larroza A, Ruiz-Espana S, Arana E, Moratal D. Classifying brain metastases by their primary site of origin using a radiomics approach based on texture analysis: a feasibility study. *Eur Radiol.* 2018; 28(11):4514-4523.

16. Shofty B, Artzi M, Shtrozberg S, et al. Virtual biopsy using MRI radiomics for prediction of BRAF status in melanoma brain metastasis. *Sci Rep.* 2020; 10(1):6623.

17. Kriegl L, Neumann J, Vieth M, et al. Up and downregulation of p16(Ink4a) expression in BRAF-mutated polyps/adenomas indicates a senescence barrier in the serrated route to colon cancer. *Mod Pathol.* 2011; 24(7):1015-1022.

18. Jenkinson M, Beckmann CF, Behrens TE, Woolrich MW, Smith SM. Fsl. *Neuroimage.* 2012; 62(2):782-790.

19. Isensee F, Schell M, Pflueger I, et al. Automated brain extraction of multisequence MRI using artificial neural networks. *Hum Brain Mapp.* 2019; 40(17):4952-4964.

20. Avants BB, Tustison NJ, Song G, Cook PA, Klein A, Gee JC. A reproducible evaluation of ANTs similarity metric performance in brain image registration. *Neuroimage.* 2011; 54(3):2033-2044.

21. Yushkevich PA, Piven J, Hazlett HC, et al. User-guided 3D active contour segmentation of anatomical structures: significantly improved efficiency and reliability. *Neuroimage.* 2006; 31(3):1116-1128.

22. Li X, Morgan PS, Ashburner J, Smith J, Rorden C. The first step for neuroimaging data analysis: DICOM to NIfTI conversion. *J Neurosci Methods.* 2016; 264:47-56.

23. Tustison NJ, Avants BB, Cook PA, et al. N4ITK: improved N3 bias correction. *IEEE Trans Med Imaging.* 2010; 29(6):1310-1320.

24. Carre A, Klausner G, Edjlali M, et al. Standardization of brain MR images across machines and protocols: bridging the gap for MRI-based radiomics. *Sci Rep.* 2020; 10(1):12340.

25. van Griethuysen JJM, Fedorov A, Parmar C, et al. Computational Radiomics System to Decode the Radiographic Phenotype. *Cancer Res.* 2017; 77(21):e104-e107.

26. Zwanenburg A, Leger S, Agolli L, et al. Assessing robustness of radiomic features by image perturbation. *Sci Rep.* 2019; 9(1):614.

27. Vallat R. Pingouin: statistics in Python. *Journal of Open Source Software.* 2018; 3(31).

28. Vuong D, Tanadini-Lang S, Wu Z, et al. Radiomics Feature Activation Maps as a New Tool for Signature Interpretability. *Front Oncol.* 2020; 10:578895.

29. Harrell FE, Jr., Lee KL, Mark DB. Multivariable prognostic models: issues in developing models, evaluating assumptions and adequacy, and measuring and reducing errors. *Stat Med.* 1996; 15(4):361-387.

30. Vittinghoff E, McCulloch CE. Relaxing the rule of ten events per variable in logistic and Cox regression. *Am J Epidemiol.* 2007; 165(6):710-718.

31. Lohmann P, Kocher M, Ceccon G, et al. Combined FET PET/MRI radiomics differentiates radiation injury from recurrent brain metastasis. *Neuroimage Clin.* 2018; 20:537-542.

32. Mouraviev A, Detsky J, Sahgal A, et al. Use of radiomics for the prediction of local control of brain metastases after stereotactic radiosurgery. *Neuro Oncol.* 2020; 22(6):797-805.

33. Tomaszewski MR, Gillies RJ. The Biological Meaning of Radiomic Features. *Radiology.* 2021; 298(3):505-516.

FIGURES & TABLES

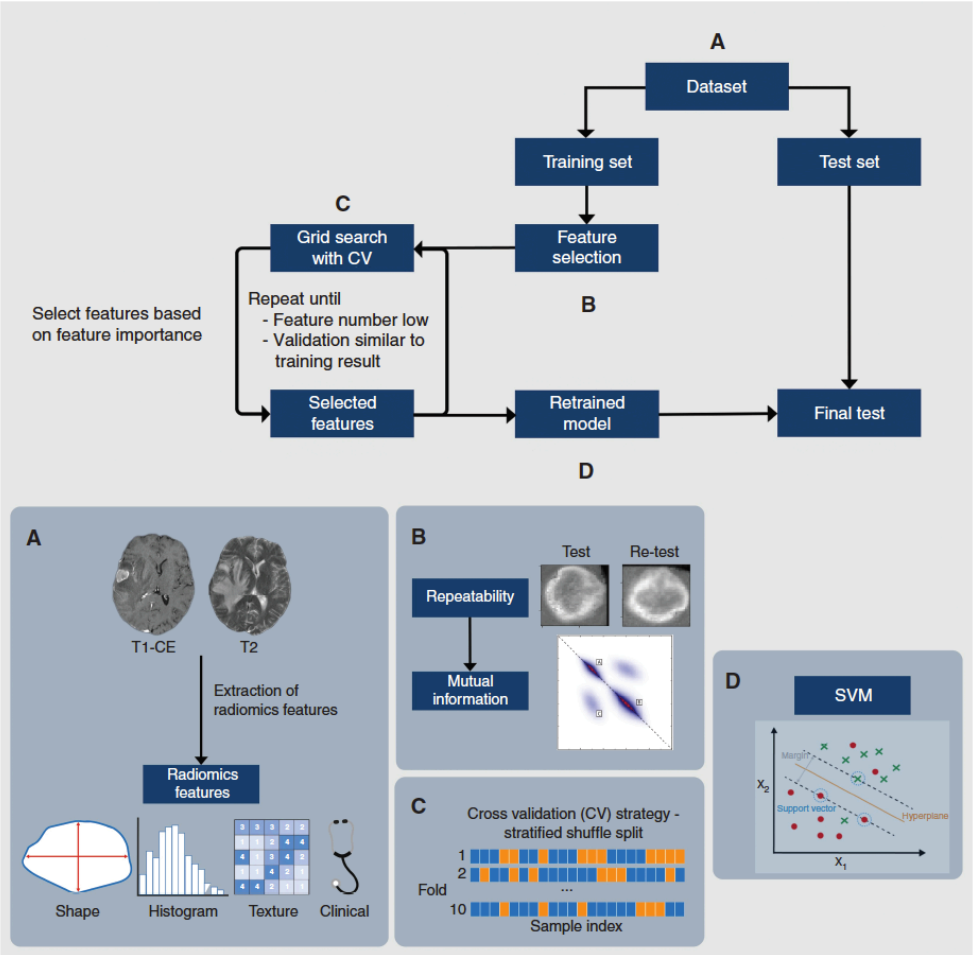

Figure 1: Radiomics workflow. a) The dataset was divided in a training set (University Hospital Cologne) and test set (University Hospital Regensburg). For both, radiomics features were extracted. b) Repeatability was calculated for features calculated on the original image and an augmented version of the image. The 100 radiomics features with highest mutual information were selected from the subset of repeatable features. c) Ten-fold stratified shuffle split cross validation was performed until the validation accuracy did not further improve. d) Using the optimal model parameters and best performing features, the model was retrained on the complete training data. In a last step the model was applied to the test set.

CV: cross validation; SVM: support vector machine; T1-CE: contrast-enhanced T1-weigted MRI; T2: T2-weighted MRI

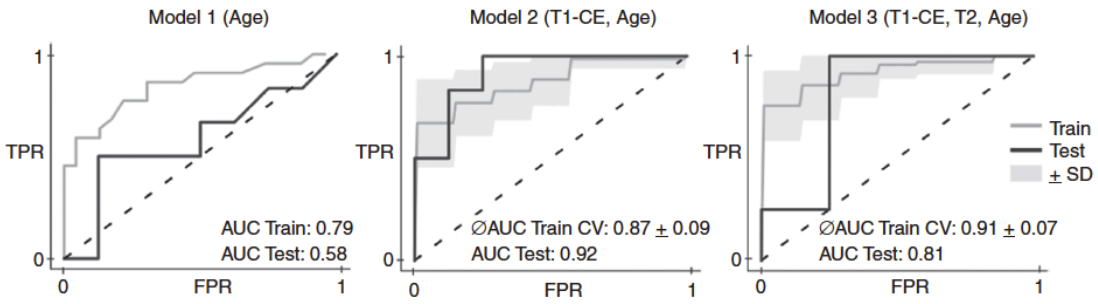

Figure 2: Receiver operating characteristic curves of the developed classifiers in the training and the test dataset.

AUC: area under the receiver operating characteristic curve; CV: cross validation; FPR: false-positive rate; SD: standard deviation; T1-CE: contrast-enhanced T1-weighted MRI; T2: T2-weighted MRI; TPR: true-positive rate

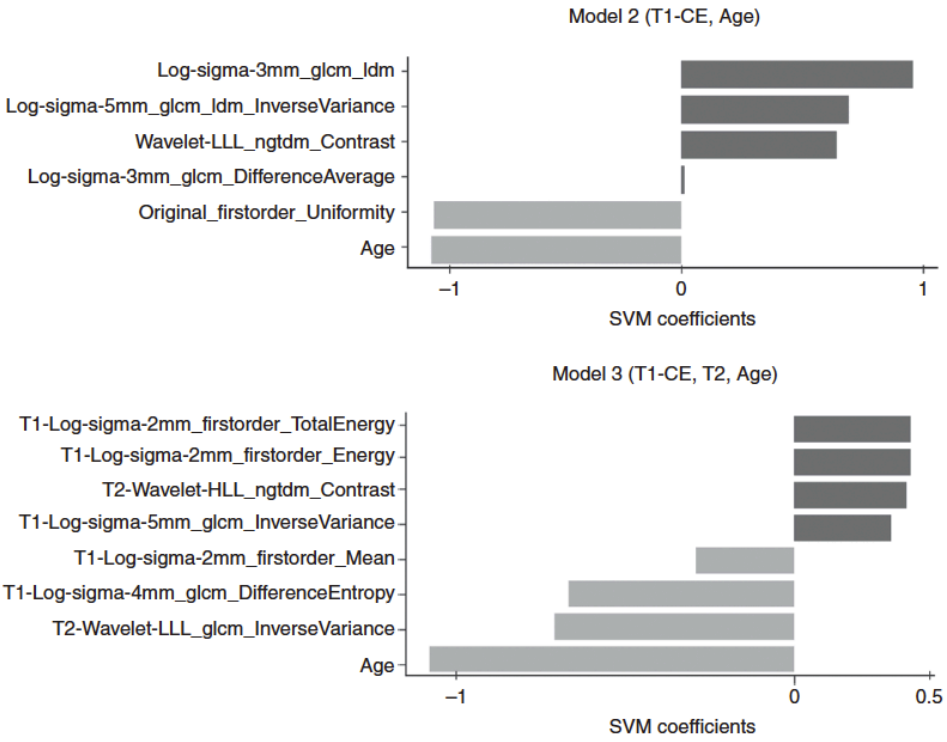

Figure 3: Feature importance expressed as support vector machine coefficients for model 2 (age + radiomics features from contrast-enhanced T1-weighted MRI) (top) and model 3 (age + radiomics features from contrast-enhanced T1- and T2-weighted MRI) (bottom). In both models, patients' age was the most important feature for the prediction of the BRAF mutation status.

glcm: gray level co-occurrence matrix; ngtdm: neighboring gray tone difference matrix; LoG: Laplacian of Gaussian; SVM: support vector machine; T1-CE: contrast-enhanced T1-weighted MRI; T2: T2-weighted MRI

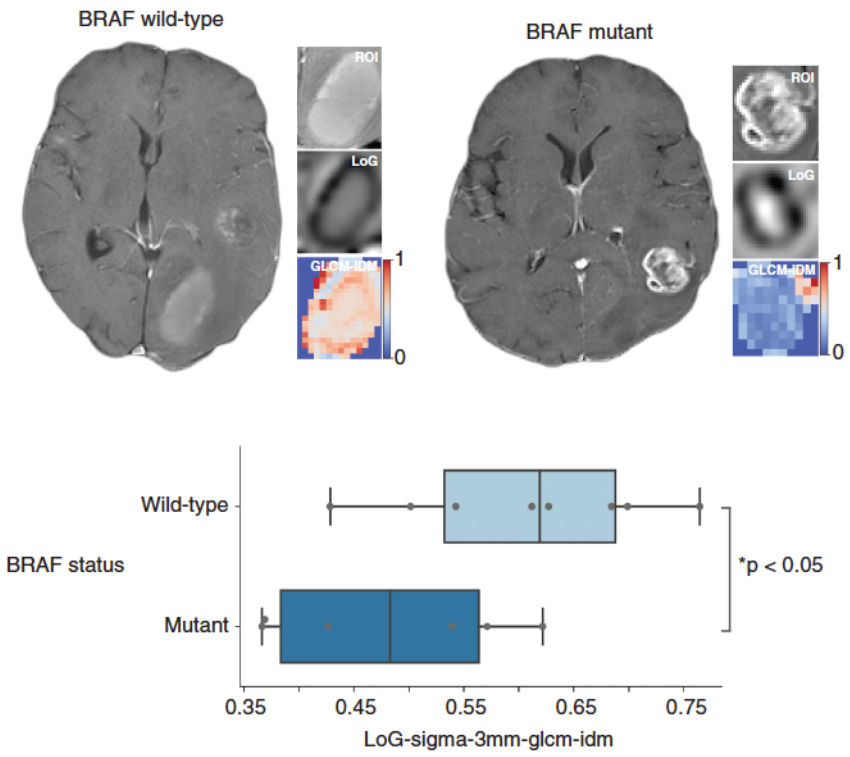

Figure 4: Visualization of different patterns of contrast enhancement in association with the BRAF mutation status. Melanoma brain metastases harboring a BRAF mutation showed a more heterogenous uptake of contrast enhancement (right), whereas BRAF wild-type melanoma brain metastases showed a more homogenous contrast enhancement (left). This visual impression is quantified by the radiomics feature inverse difference moment of the grey level co-occurrence matrix (GLCM-IDM). This feature reflects the local image homogeneity and showed statistically significant higher values for BRAF wild-type melanoma brain metastases compared to BRAF mutant tumors (Box plot, bottom).

LoG: Laplacian of Gaussian image filter; ROI: region-of-interest

Table 1: Patient characteristics.

	Training Set – Cologne (n=45)			Test Set – Regensburg (n=14)		
	Total	BRAF wild-type	BRAF mutant	Total	BRAF wild-type	BRAF mutant
Number of patients	45	23	22	14	6	8
Sex (female/male)	21/24	11/12	10/12	6/8	4/2	2/6
Age at surgery (years) (mean ± sd)	60 ± 12	60 ± 12	59 ± 12	59 ± 11	67 ± 8	53 ± 8
Number of patients with						
singular	26	14	12	5	4	1
2-3	10	5	5	3	1	2
more than 3 metastases	9	4	5	6	1	5
Tumor volume (ml) (mean ± sd)	19.0 ± 13.3	19.8 ± 11.7	18.1 ± 14.9	14.2 ± 14.3	20.3 ± 16.3	6.0 ± 4.5
Intrametastatic hemorrhage	26	13	13	3	1	2
Cystic tumor	7	2	5	3	3	0
Karnofsky performance score preoperative (median) (range)	90 (20-100)	90 (20-100)	90 (30-100)	90 (20-100)	80 (20-100)	90 (30-100)
Time to detection of brain metastases (months) (mean ± sd)	57 ± 69	56 ± 70	50 ± 63	64 ± 76	25 ± 27	98 ± 87
Location						
- temporal left/right	5/4	2/3	3/1	1/2	0/1	1/1
- parietal left/right	3/4	1/2	2/2	3/1	2/0	1/1
- frontal left/right	5/13	2/6	3/7	0/1	0/0	0/1
- cerebellar left/right	5/3	5/1	0/2	1/1	0/1	1/0
- central left/right	1/0	1/0	0/0	0/0	0/0	0/0
- occipital left/right	1/1	0/0	1/1	0/1	0/1	0/0
Previous systemic therapy (multiple possible):						
- Chemotherapy	5	4	11	5	3	2
- Immunotherapy	22	10	12	13	6	7
- Targeted therapy	17	7	10	8	0	8
- Interferon therapy	16	7	9	3	2	1

Table 2: **Top** - Results from 10-fold stratified cross validation of model 2 (age + radiomics features from contrast-enhanced T1-weighted MRI) and model 3 (age + radiomics features from contrast-enhanced T1- and T2-weighted MRI) using the data set from the University Hospital Cologne. **Bottom** - Test results of model 2 and model 3 using the independent data set from the University Hospital Regensburg.

Acc: accuracy; AUC: area under the receiver operating characteristic curve; CV: cross validation; SD: standard deviation; Sens: sensitivity; Spec: specificity; T1-CE: contrast-enhanced T1-weighted MRI; T2: T2-weighted MRI

TRAINING								
	Model 2 (T1-CE, age)				**Model 3 (T1-CE, T2, age)**			
CV fold	Acc [%]	AUC	Sens [%]	Spec [%]	Acc [%]	AUC	Sens [%]	Spec [%]
1	100.0	1.00	100.0	100.0	92.9	0.96	85.7	100.0
2	71.4	0.78	71.4	71.4	78.6	0.78	57.1	100.0
3	85.7	0.84	71.4	100.0	92.9	0.94	100.0	85.7
4	85.7	0.92	85.7	85.7	92.9	0.98	85.7	100.0
5	71.4	0.76	57.1	85.7	78.6	0.86	85.7	71.4
6	78.6	0.88	71.4	85.7	92.9	0.98	85.7	100.0
7	92.9	0.96	85.7	100.0	100.0	1.00	100	100.0
8	78.6	0.76	57.1	100.0	85.7	0.86	85.7	85.7
9	85.7	0.86	85.7	85.7	78.6	0.84	71.4	85.7
10	100.0	1.00	100.0	100.0	100.0	1.00	100.0	100.0
Mean ± SD	**85.0 ± 10.3**	**0.87 ± 0.09**	**78.5 ± 15.4**	**91.4 ± 0.09**	**83.5 ± 10.1**	**0.92 ± 0.08**	**85.7 ± 13.4**	**92.8 ± 10.1**
TEST								
	Model 2 (T1-CE, age)				**Model 3 (T1-CE, T2, age)**			
	Acc [%]	AUC	Sens [%]	Spec [%]	Acc [%]	AUC	Sens [%]	Spec [%]
	86.0	**0.92**	**83.0**	**88.0**	**88.0**	**0.81**	**100**	**75.0**